ISSN 2075-1087, Gyroscopy and Navigation, 2024, Vol. 15, No.2, pp. 3-20
Russian Text © The Author(s), 2024, published in Giroskopiya i Navigatsiya, 2024, No.2, pp. 8-34.

Light Sources for Fiber-Optic Gyroscopes

D. A. Egorov[a,*], Ye. L. Klyuchnikova[a], A. A. Untilov[a], A. S. Aleinik[b], S. A. Volkovskii[b], V. N. Kuznetsov[b], V. S. Oshlakov[b], G. K. Pogudin[b], and L. B. Liokumovich[c]

[a]*Concern CSRI Elektropribor, JSC, St. Petersburg, Russia*,
[b]*ITMO University, St. Petersburg, Russia*,
[c]*Peter the Great St. Petersburg Polytechnic University*
*****e-mail: egorov_da@mail.ru*
Received February 22, 2024; reviewed May 6, 2024; accepted June 27, 2024

Abstract: The light source is one of the key components of fiber optic gyroscopes (FOGs) since its optical parameters determine FOG performance, including the scale factor and zero bias stability. In this paper we consider the main types of light sources that are most suitable for FOGs. We describe their design principles and relevant technical characteristics, review commercially available light sources, and provide a brief assessment of the prospects for the development of light sources in the context of fiber optic gyroscopy.

Keywords: light sources, spectral characteristics, fiber optic gyroscope (FOG), scale factor stability.

1. INTRODUCTION. GENERAL PROVISIONS

Over the last decades, one of the important lines of research and development in the field of fiber optics for navigation, positioning, orientation, stabilization and motion control applications has been the development of FOGs, which are a serious competitor to traditional mechanical and laser gyroscopes due to their high reliability, wide dynamic range, long service life, low power consumption, light weight, and low cost [1, 2].

The FOG operating principle is based on the Sagnac effect in a ring interferometer, which is well known [2]. The essence of this phenomenon lies in the fact that when the fiber-optic ring interferometer (FRI), or Sagnac interferometer, rotates with an angular rate of Ω, its optical waves, propagating in counter directions, produce a Sagnac phase difference Δφ specified by equation [2]

$$\Delta\varphi = \frac{4\pi R L}{\lambda c}\Omega, \qquad (1)$$

where λ is the wavelength of the light source (LS), m; c is the speed of light in vacuum, m/s; R is the FRI coil radius, m; L is the coil length, m.

The Sagnac effect is relativistic, which is why in order to provide for an acceptable level of sensitivity and measurement of small angular rates Ω, the FRI is based on a multiturn coil, thus making it possible to proportionally enlarge the area of the fiber coil while maintaining relatively small values of the radius R and the dimensions of the device as a whole. The FRI is self-consistent since in the absence of nonstationary effects on the coil, the interfering counterpropagating waves travel the same path and have the same phase shift. Though the presence of nonstationary effects on the coil, mainly temperature, results in the appearance of a component in the phase difference of the interferometer that is not related to the angular rate, it does not create fundamental limitations for this method of measurement. Such effects can be minimized due to special techniques for FRI winding as well as software compensation methods. All this made it advantageous to use FRI for FOGs [2,3].

The working point of the FOG interferometer is shifted from the region of maximum of the harmonic interference function to a more linear section, which becomes possible owing to a special auxiliary modulation of the argument of interference oscillations and special processing of the interferometer signal. This allows the phase difference Δφ to be determined with high accuracy and good resolution over a wide range of angular rates [2].

Fundamental limitations on the resolution of measuring the phase difference Δφ and, as a consequence, the angular rate Ω are associated with the

signal-to-noise ratio obtained in the interference signal, but in practice, we can observe additional fluctuations and distortions of the interference signal in the FRI that adversely affect the result of the Sagnac phase difference measurement. A significant factor leading to parasitic disturbances in the FRI signal is the emergence of various additional paths of wave propagation in the fiber coil and additional interference components that are not related to the angular rate Ω. Such paths arise due to the propagation of light in a fiber coil in the form of different polarization modes in the presence of mode coupling, due to light scattering in the fiber and the interaction of counterpropagating waves, due to spurious reflections from fiber connections and from the elements of the circuit. The negative impact of such effects can be partially mitigated by the configuration and fine tuning of the optical circuitry, but their parasitic influence remains significant. Parasitic interference components caused by the above-mentioned effects are also observed in fiber-optic interferometers of another type, which have orders of magnitude shorter fiber length and directly detect the impact-induced change in the optical length. For this reason, the influence of weak additional interference components is usually not as important for them as for FRI-based FOGs.

On the other hand, taking into consideration the specifics of the Sagnac interferometer as a self-consistent device, all parasitic interference components are significantly suppressed by weakly coherent LS with a relatively wide spectrum, which has become the main generally accepted approach in this case. Interference oscillations remain only for waves that have passed strictly identical optical paths, which eliminates interference of the majority of spurious optical waves and suppresses distortions during measuring the Sagnac phase difference [4]. The use of such LS makes it possible to reduce the requirements for the reflections in connections and circuit elements, for the extinction of the used polarizers and other parameters of the elements associated with the emergence of parasitic light propagation paths in the interferometer coil [2].

The purpose of this work is to review and analyze the main types of LS suitable for FOGs, and to briefly describe the design principles and technical characteristics of the sources that are most important for this application. The paper also provides a review of commercially available LS, brief assessment of the prospects for the LS development in the context of fiber-optic gyroscopy, and recommendations for choosing LS depending on the FOG's field of application.

2. LS KEY CHARACTERISTICS FOR CONSTRUCTING A FOG

If we rank all the characteristics of LS by significance in the context of their application to FOG, the stability of the spectrum and its width should be considered of primary importance. The requirements for spectrum stability are determined by the fact that λ is directly included into relation (1). A wide spectrum and, as a consequence, a short coherence length are necessary to suppress components in the FOG interference signal that are not related to the angular rate Ω. Minor, yet also important characteristics, are the LS output power, which affects the signal-to-noise ratio of the interference signal, as well as the polarization properties of the source—the degree of polarization and orientation of the polarization axes—which must be taken into account when constructing FOG optical schemes to mitigate unwanted interactions of polarization modes.

Weighted average of LS wavelength and its spectral width

To activate a broadband LS, it is necessary to specify the parameter λ in formula (1). In the case that the LS spectrum of the source $S_P(\nu)$ (here S_P is the spectral density of optical power, W/Hz; ν is the optical frequency, Hz) is symmetric with respect to the central frequency ν_0, it is correct to use the value of the central wavelength $\lambda_0 = c/\nu_0$ in formula (1). Real sources may have complex asymmetric spectra, and in general, weighted mean values should be used, which are determined by relation [5]:

$$\lambda_{wa} \approx \frac{c}{\nu_{wa}} = c \cdot \left(\frac{\int \nu \cdot S_P(\nu) d\nu}{\int S_P(\nu) d\nu}\right)^{-1}, \qquad (2)$$

where ν_{wa} is the weighted average frequency, which is given by the expression in parentheses, and λ_{wa} is the weighted average wavelength (WAW). For a symmetric spectrum $\nu_{wa} = \nu_0$ and $\lambda_{wa} = \lambda_0$.

The WAW directly specifies the FOG scale factor (conversion factor) in accordance with (1), and its shift by $\delta\lambda_{wa}$ leads to an erroneous shift of $\delta\Omega$ of the measured angular rate value:

$$\delta\Omega = \frac{\Omega}{\lambda_{wa}} \cdot \delta\lambda_{wa}. \qquad (3)$$

Fluctuations in λ_{wa} can be caused by changes in the spectrum shape, including those caused by temperature effects and LS aging. For a navigation-grade FOG, the required stability of the WAW is 1 ppm, taking into account the influence of all destabilizing factors, among which are the temperature of the semiconductor structure, LS pump current, and others.

The LS spectral width is also generally characterized using the root-mean-square (rms) value of the width [5]:

$$\Delta\nu_{\text{rms}} = \sqrt{\frac{\int(\nu-\nu_{wa})^2\cdot S_P^2(\nu)d\nu}{\int S_P^2 d\nu}}. \quad (4)$$

In the case of simple and, particularly, symmetric $S_P(\nu)$ dependencies, the spectral width is often given, determined by a specified level of S_P decrease relative to the maximum value. The relationship of such estimates with the rms width depends on the spectrum shape. If, for example, $S_P(\nu)$ is described by a Gaussian curve with variance σ in the form $S_P(\nu) \sim \exp[-(\nu - \nu_0)^2/4\sigma^2]$, then from (2) and (4), we obtain $\Delta\nu_{\text{rms}} = \sigma$, and the commonly used full width at half maximum (FWHM) (i.e. –3 dB) will be equal to $3.33\cdot\Delta\nu_{\text{rms}}$.

Also, it should be noted that in most cases, the devices for measuring the LS spectrum measure the S_P dependence on the wavelength, i.e., the LS spectrum is recorded in the wavelength scale. In this case, to apply formulas (2) and (3), we need to recalculate the $S_P(\lambda)$ dependence into the $S_P(\nu)$ spectrum using the relation $\lambda = c/\nu$ for the argument, and also taking into account the relation $\delta\nu = \delta\lambda\cdot c/(\lambda^2)$ for the spectrum analyzer filter bandwidth when recalculating the S_P level. The spectral width at the ½ maximum level for LS in a navigation-grade FOG should be no less than 5 nm [11]; most of the commercially available LS of suitable types have spectral widths in the range of 30–80 nm.

LS temporal coherence

Another important characteristic, which takes into account the LS nonmonochromaticity and suppression of the influence of interference of the waves traveling through different optical paths, is LS temporal coherence. If the beam of an optical source is split into two waves that travel through two paths with a difference ΔL and then combine, the interference oscillations of the optical power caused by the changes in ΔL will be described by formula [2]:

$$P(\Delta L) = \frac{P_0}{2}\left[1 + \gamma_{ce}(\Delta L)\cos\left(2\pi\frac{\Delta L\cdot n}{\lambda_{\text{wa}}}\right) + \gamma_{co}(\Delta L)\sin\left(2\pi\frac{\Delta L\cdot n}{\lambda_{\text{wa}}}\right)\right], \quad (5)$$

where P_0 and λ_{wa} are the power and LS WAW, n is the refractive index of the medium in which the interfering waves are split and combine.

Formula (5) is written under the assumption that the interfering waves have the same amplitudes and the same polarization states, so that there is no need to introduce additional coefficients to take into account such mismatches. When considering interference oscillations (5) in relation to the case of a self-consistent Sagnac interferometer, the equivalent path difference is $\Delta L = 2R\cdot L\cdot\Omega/c$. The decrease in the amplitude of interference oscillations with increasing ΔL is determined by the coherence function [6], represented in (5) by the even $\gamma_{ce}(\Delta L)$ and odd $\gamma_{co}(\Delta L)$ components, which are associated with the LS spectrum. In the case of a symmetric spectrum, there is no odd component, but even for an asymmetric spectrum, the contribution of the odd component is usually small, and it is neglected in the quantitative estimation of the coherence function.

The faster the LS coherence function decreases with the ΔL increase and the lower is the level of oscillations of this function (the presence and size of the so-called "side lobes" of the function – secondary, or side, maxima), the less is the existence of parasitic interferometric components in the real coil of the FOG ring interferometer [7]. The larger is the LS $\Delta\nu_{wa}$, the faster is the general decline in the coherence function; and the features of oscillations of the dependences $\gamma_{ce}(\Delta L)$ and $\gamma_{co}(\Delta L)$ are associated with the specific shape of the LS spectrum (the coherence functions of some commercially available LS are given in Section 5).

For LS used in FOGs, the most informative are the coherence length Lc and decoherence length Ldc determined by the levels of the coherence function – 0.8 and 0.03, respectively (Fig. 1). The Ldc value for LS should not exceed a few millimeters and for the majority of suitable sources, it is in the range from 30–50 μm (for superluminescent diodes) up to 300–500 μm (for erbium superluminescent sources).

In practice, LS are usually characterized by power spectrum $S_P(\lambda)$. This characteristic is easier to measure because the instruments for measuring the optical spectrum are available. It is the power spectra that manufacturers usually provide in LS data sheets. If necessary, the components of the coherence function $\gamma_{ce}(\Delta L)$

and $\gamma_{co}(\Delta L)$ can be obtained from the analysis of the LS spectrum shape using the inverse Fourier transform [2, 7]. Such an estimation can be useful, for example, in a comparative analysis of different LS, in targeted modification of the LS spectrum, and in other practical scenarios.

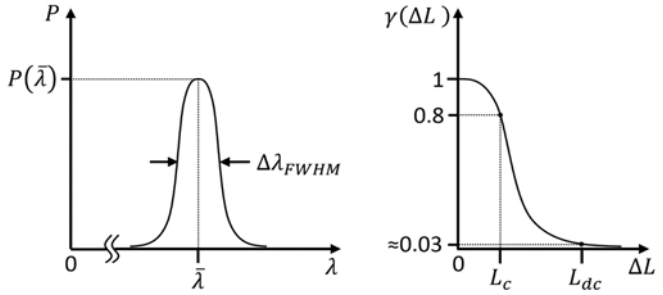

Fig. 1. LS spectrum and its coherence function, $\Delta\lambda_{FWHM}$ is a spectrum width at half-height [6].

The influence of the spectrum shape on measurement errors Ω cannot be described in simple explicit expressions, all the more so because this influence may depend on the algorithm for processing the interference signal, and other factors. It is clear that an optical source with a wider symmetric Gaussian-like spectrum is preferable in terms of the FOG accuracy characteristics. Small coherence and decoherence lengths, as well as the absence of "side lobes" indicate that the energy of the parasitic interference components of such LS is insignificant. It is also clear that in the comparison of two LS with similar spectra, preference should be given to the one that has the smallest L_c, L_{dc} and "lobe" height; however, for a strict comparison of two LS, the first of which, for example, has a wider but less symmetric spectrum, a numerical analysis of signal formation and processing in a circuit with a ring interferometer is needed, taking into account the LS spectrum. Such studies for LS most commonly used in FOGs (with different spectral shapes) should be a subject-matter of a separate research.

LS output optical power

The absolute level of output optical power P_0, which determines the level of the interference signal and the resulting signal-to-noise ratio limiting the resolution of Sanyak phase and angular rate measurements, is also an important LS characteristic in the context of FOG applications. As P_0 increases, the role of noise of the electronic detection circuitry and the contribution of shot noise decrease [8]. Also, with sufficiently high output power, an LS can be used to ensure the operation of several FOGs as part of navigation modules, usually containing three or four gyroscopes with different orientations of the sensitivity axes of fiber-optic coils.

The range of LS optical power values for FOGs is rather wide; devices with a relatively short coil (up to 1 km) can be built using sources with a power of about 1 mW; however, a high signal-to-noise ratio in high-precision devices (coil length of 1 km or more) can be provided with LS that have an output optical power of 10 mW or more.

It should also be noted that as the optical power of LS and the energy density in the fiber increase, the error caused by the nonlinear Kerr effect also increases in the FOG output signal. The contribution of this error can be substantially decreased when a wide-spectrum LS is used in the FOG [2].

Relative intensity noise

A parameter closely related to the LS optical power is the level of relative intensity noise (RIN), which is usually given in decibels relative to the optical power at the LS output. This parameter characterizes the level of random fluctuations in the LS output optical power caused by a number of factors, in particular, thermal fluctuations of the active medium and some others.

A type of RIN for a wide-spectrum LS is excess RIN (ERIN) caused by random fluctuations in the optical power of different spectral components. ERIN is one of the main LS parameters that limits the signal-to-noise ratio of the FOG optoelectronic circuit and, as a result, increases the angular random walk (ARW). Since the spectral power density of ERIN is inversely proportional to the spectrum width, this effect is higher for LS with a narrower spectrum. It should be noted that there are quite a few known techniques to reduce the influence of ERIN on the FOG performance at the levels of both the optical circuitry and signal processing algorithms [9, 10]. In most high-precision FOGs with broadband LS, the application of one or more methods can reduce the ERIN contribution to the interferometer phase error to the level of shot noise.

LS polarization properties

When designing high-precision FOGs, it is necessary to take into account the polarization properties of all components included in the optical circuit and the connections between them. Polarization transformations are one of the reasons for the violation of the Sagnac interferometer reciprocity and the appearance – in the output FOG signal – of the components

associated with the interference of different polarization modes rather than with the angular rate. One of the two approaches is most often used to suppress such components: constructing an interferometer coil from a fiber while maintaining polarization, and constructing a coil from a standard optical fiber together with depolarization of the incoming and outgoing beams [2].

In both cases, it is preferable to use an unpolarized or depolarized LS so that polarizers are further used in the optical circuit. In this case, there is no need to match the polarization modes of the LS fiber output and the interferometer fiber coil. It is easier to get radiation with high extinction than generate and maintain high stability of the polarization state at the LS output. The use of a polarizer and polarization-preserving fiber in the optical design makes it possible to somewhat relax the requirements for a low degree of LS polarization, but for high-precision devices, this value should not exceed 1%.

Table 1 summarizes and describes the most significant characteristics of the LS for FOG applications.

Table 1. The main characteristics of LS used in FOGs

Characteristics	General requirements/mechanism of influence
Output optical power (in fiber)	▪ The higher the power, the higher the FOG signal-to-noise ratio ▪ Too high power – danger of nonlinear effects in the fiber ▪ High power allows several interferometers to be served by a single source ▪ The minimum power level is determined by the FOG parameters: loop length, processing circuit parameters, and others. The conditional minimum is ≈10 mW
FWDM	▪ The wider the spectrum, the shorter coherence length and smaller contribution of parasitic interference components to the FOG signal ▪ For a navigation-grade FOG, the conditional minimum limit is ≈5 nm [11]
Spectrum shape	▪ The closer the spectrum to the Gaussian shape, the lower the energy of the parasitic interference components
WAW stability	▪ WAW is included in the FOG scale factor. For a navigation-grade FOG, long-term stability ▪ of the WAW should be of the order of 1 ppm [12]
Coherence function form, coherence length (L_c),	▪ For FOGs, LS with a minimum length Lc and the absence of "side lobes" are preferable ▪ If the coherence functions have similar forms, the preference should be given to LS ▪ with the shortest coherence length and the minimum height of the "side lobes" ▪ If the coherence functions differ significantly in their forms, numerical simulation or a comparative experiment should be carried out for a correct comparison
Excess relative intensity noise (ERIN)	▪ Increase in ERIN leads to an increase in FOG ARW ▪ The wider the spectrum, the smaller the ERIN ▪ There are effective techniques to decrease ERIN
Output polarization	▪ For high-accuracy FOGs, LS with unpolarized or depolarized radiation are preferable ▪ The use of a polarizer in the FOG circuit reduces the input optical power, but minimizes the negative effects associated with the LS polarization

3. MAIN TYPES OF LS SUITABLE FOR FOGS

LS with WAW at about 850 nm, i.e. in the so-called first transparency window of quartz optical fibers, are often used for tactical-grade FOGs with the length of a ring interferometer coil of less than 1 km. In the case of extended fiber optic coils for navigation-grade FOGs (1 km or more), LS with WAW in the region of 1550 nm are relevant; this is the so-called C-band or the third transparency window, where optical power losses in quartz optical fibers are minimal. A decrease in the interferometer sensitivity due to an increase in the WAW can be compensated for by multiple lengthening of the fiber optic coil [2].

Despite their wide spectrum, light-emitting diodes (LEDs) have not become effective sources for FOGs because they cannot provide either sufficient levels of optical power in the optical fiber or operation in the C-band.

Laser sources are also not widely used in FOGs, since they have a discrete and too narrow spectrum, although a number of studies in recent years have demonstrated that they are potentially applicable both in tactical-grade FOGs and in more precise devices, in which case their spectrum is broadened in various ways.

The most attractive and promising today are two types of LS which are based on the effect of amplified spontaneous emission (ASE) or superluminescence, with the operating wavelength of 1550 nm and a rela-

tively wide spectrum. These are superluminescent diodes (SLDs) [13–15] and superfluorescent (also often called superluminescent in Russia) fiber sources (SFS), most often implemented on active erbium fiber (hereinafter referred to as erbium superluminescent sources (ESS)) [8, 16–18].

In the following sections, we consider the abovementioned sources in more detail.

4. SUPERLUMINESCENT DIODES (SLD)

SLDs are a double heterostructure of an active layer between the layers of p-type and n-type semiconductors formed on an n-type substrate. Their structure is similar to that of laser diodes, with one exception – SLDs do not have resonator mirrors (Fig. 2); instead, an antireflection coating is often applied to the emitting side, while the opposite side is cleaved at an angle and/or a layer of absorbing material is applied. Ideally, spontaneous emission resulting from the application of a potential difference to the electrodes passes through the active region only once; so, it is not specific modes that are amplified, which is typical for a system with a resonator, but all wavelengths corresponding to the parameters of the heterostructure [19].

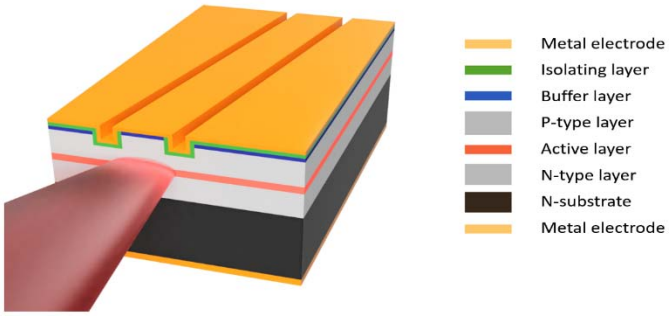

Fig. 2. Simplified structure of an SLD-type LS with a comb waveguide and end surfaces beveled to suppress resonance

Serially produced SLDs have an active length of about 300–500 μm. The semiconductor structure is placed in a housing with subsequent sealing; an optical fiber is connected to the SLD from the output side of the active zone. The level of optical power injected into the fiber is usually between a few and tens milliwatts; the efficiency of introducing radiation into the fiber is 10–20%. In this parameter, SLDs are comparable to laser diodes—SLDs also have a high degree of spatial coherence, but they differ from laser diodes in a significantly wider emission spectrum.

Since the operating principle of SLDs is based on the generation and amplification of spontaneous emission, the shape and substances used in the crystal composition directly affect the parameters of the resulting radiation. In particular, for different polarization modes, the gains may be different in certain types of the active layer material. LS that are most commonly used for FOGs have a wavelength of 1550 nm; in SLDs, for this spectral range, InGaAlAs is usually used as an active medium material, which is characterized by a significant dependence of the gain of spontaneous emission on its polarization. Thus, the resulting SLD radiation has elliptical polarization—about 70–80% of the radiation power is polarized parallel to the plane of the active region.

Most of commercially available SLDs with a Gaussian spectral shape have FWHM of 30 nm (the spectra of such SLDs are considered below). In high-power SLDs, pulsations in the power spectral density can be observed, typically, in the vicinity of the peak wavelength. Such pulsations are explained by the presence of residual reflections from the ends of the chip and from the end of the fiber. The main countermeasure against this phenomenon is antireflection coating of the fiber and diode surface.

The main difficulty in using SLD in FOGs is a relatively low stability of the spectrum and WAW shift both under the influence of temperature variations (about 400 ppm/°C) and fluctuations of the control current (about 40 ppm/mA) [2]. Active thermal stabilization of the semiconductor structure, power supply with highly stable current and other technical measures make it possible to stabilize WAW to approximately 150 ppm in the temperature range from –40 to +60°C [20].

A limiting factor is also the change in SLD parameters as a result of aging, particularly at elevated temperatures in the region of the semiconductor structure. This effect is mainly manifested as a change in the output optical power, more often decrease than increase. Physical mechanisms of degradation are currently a relevant area of research; more than 10 mechanisms have been described in various reviews [20–22]. The negative contribution of such effects can be partially minimized by using such additional compensation mechanisms as thermal stabilization, precision current sources, optical power feedback, and others [13,17,23,24]; however, to achieve WAW stability to better than 100 ppm is still technically challenging.

In the context of their application in FOGs, SLD-type sources are suitable for devices that are subject to increased requirements in terms of reduced weight, size, and final cost. SLD can be used directly as part of

an integrated optical module together with other optical components of the FOG circuitry, which makes it possible to achieve minimum dimensions of the final device [25, 26]. On the other hand, the relatively low stability of WAW and changes of characteristics due to aging limit the application of SLDs in FOGs intended for high-precision navigation devices and complexes.

Among the FOG-manufacturers using SLD are the Research and Production Company Optolink, JSC Physoptika (both Russia), and KVH (the USA) [27–29].

5. SUPERLUMINESCENT FIBER LS

Another type of LS often used for FOGs are superfluorescent (superluminescent) fiber sources, which use the phenomena of forced and spontaneous emission, and optical fibers doped with rare-earth elements, neodymium or erbium, as the active medium. Erbium fiber-based ESS are most often used in FOGs since the emission spectrum of such ESS fits to the C-band.

A minimum ESS circuit includes a pump laser diode and an erbium-doped active fiber. Light generation in the active fiber is based on the circuit of energy levels of erbium ions presented in Fig. 3a in a simplified form. Due to the interaction of erbium ions with the intracrystalline field of quartz glass (Stark effect), each of the erbium energy levels is split into sublevels (multiplets). Under the action of pumping photons, erbium ions pass from the ground state 4I15/2 to the metastable level 4I13/2 or to the upper excited state 4I11/2, later moving to the metastable level as a result of relaxation processes.

Ions from the metastable level pass to the ground state both spontaneously and under the influence of pumping, which results in the generation of superluminescence at wavelengths in the range of 1520–1570 nm in two opposite directions. The quantity of ions involved in the superluminescence generation increases with the increase in pumping optical power, and, largely, due to interaction of already generated photons with the ions at the metastable level. Optical pumping is carried out at wavelengths of 980 and 1480 nm. Pumping at 1480 nm has a higher quantum efficiency, but at the same time, a higher noise factor as compared to pumping at 980 nm [7].

There are single-pass and double-pass active fiber pumping circuits. In single-pass circuits, part of the superluminescence generated in the active fiber under the action of pumping radiation is not used, while in double-pass circuits, Fig. 3b, a reflector is installed in one of the ESS branches. The efficiency of double-pass circuits with double-sided pumping, incorporating unpumped erbium fiber (to broaden the spectrum of the fiber-optic source), depends on the length of this fiber; it is about 45–50%.

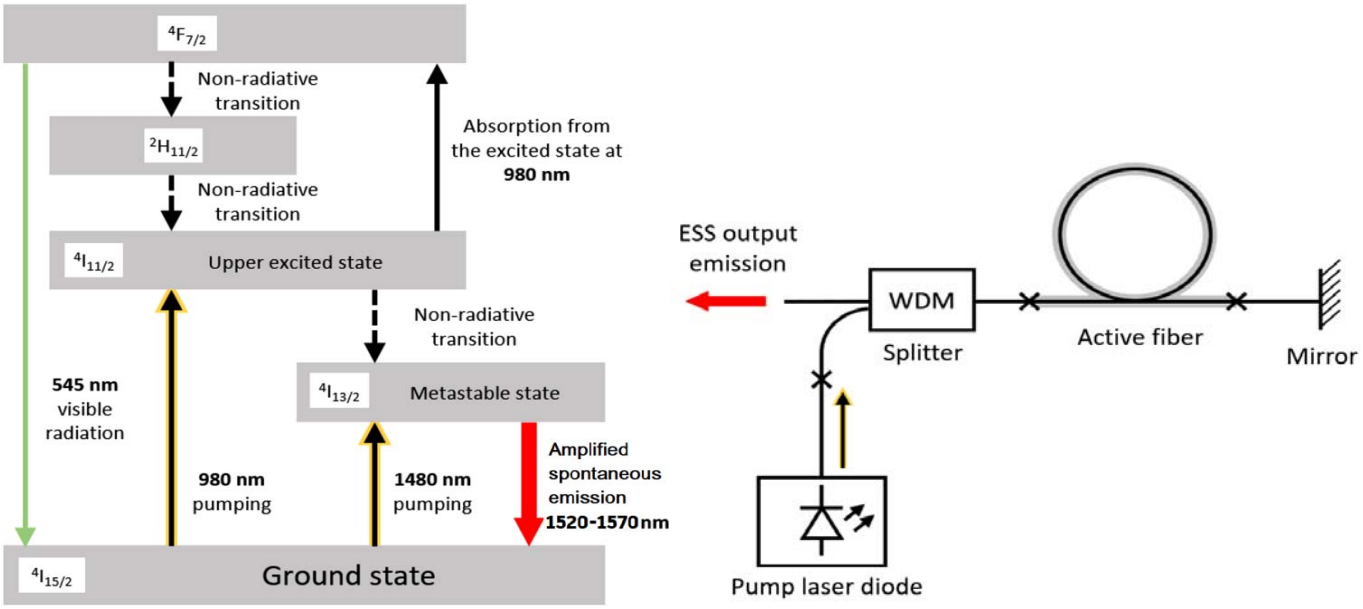

(a) *(b)*

Fig. 3. (a) Energy levels of Er3+, (b) a double-pass pumping scheme for erbium fiber with counter-directional pumping.

A large number of works analyze and compare ESS performance in different configurations [11,18,30,31]. Based on the available results, it can be concluded that circuits with counter-directional pumping have the

lowest intensity noise and higher stability of parameters; as for their use in FOGs, from the point of view of noise in the output signal, a double-pass circuit with counter-directional pumping is most effective.

The power of most commercially available C-band ESS varies from 10 to 80 mW. The FWDM can reach 80–100 nm (30–50 nm on average), and the spectrum shape usually differs significantly from the Gaussian one (spectra of commercially available ESS are discussed below). As in the case with SLDs, in ESS optical circuits, there is a possibility of narrow-band lasing due to backward reflections from the ends of the fibers, as well as from optical devices connected to the external port. To prevent this, the ends of the fibers are terminated and a fiber-optic isolator is used at the circuit output.

The ESS output light is initially not polarized because of the isotropic nature of the spontaneous emission. Since only one polarization mode is used in the FOG circuit, a polarizer is placed at the output of such an ESS, which leads to a double drop in the LS output optical power.

There are also ESS schemes that make it possible to obtain polarized light; for this purpose, polarizers are installed in the circuit and special components are used to preserve the polarization of the radiation [32]. On the contrary, to reduce the residual polarization in ESS, the radiation of pumping laser diodes is depolarized, and a Lyot depolarizer is installed at the output of the ESS optical circuit; also, a Faraday mirror is used in two-pass circuits.

Since the energy levels of rare-earth atoms are much more stable than those of semiconductors, ESS have more stable WAW, which is one of the main advantages of LS of this type when used in FOGs. For commercially available ESS, the WAW temperature coefficient varies from 2 to 200 ppm/°C depending on the operating temperature range and the spectral range of the output light. Thus, ESS with WAW at the wavelength of about 1530 nm have a more temperature-stable optical spectrum compared to ESS with WAW at a wavelength of about 1560 nm [33,34].

Thus, to increase the WAW temperature stability, it is advisable to include ESS filters in the optical circuit to reduce the contribution of spectral components, the energy of which has a notable temperature dependence [35]. In addition, filters (for example, those based on long-period fiber gratings [36]), suppress part of the output spectrum, making its shape close to the Gaussian one.

Currently, ESS are used in navigation-grade FOGs from such manufacturers as Concern CSRI Elektropribor, Perm Research and Production Instrument-Making Company (both Russia), Exail (former iXBlue), Northrop Grumman, and others [37–40].

In Table 2, we compare SLD and ESS in terms of the key parameters as applied to FOGs. The information provided is relevant to the majority of commercially available LS. It should be noted that in some publications we can come across information on devices with significantly different performance; they are often experimental and/or modified LS of one of the two given types.

Table 2. Comparison of SLD and ESS key parameters with regard to the application in to FOGs

Parameter	SLD-type LS	ESS-type LS
Output optical power (in fiber)	Units–tens mW	Tens-a few hundreds mW
	NOTE Both types of LS have an output power sufficient for use in high-precision FOGs; ESS is on average more powerful	
FWDM	30–80 nm	30–50 nm
	NOTE Both types of LS have a sufficiently wide spectrum	
Spectrum shape	Close to Gaussian	Complicated
	NOTE ESS spectrum shape can be brought closer to the Gaussian one, but this requires complication of the optical circuit and affects other parameters of LS, for example, it reduces the output optical power	
WAW stability over operating temperature range	About 100 ppm or more	About 1 to10 ppm
	NOTE A more stable WAW value is the main advantage of ESS and one of the main reasons for their wider use in high-precision FOGs	
Coherence function form, coherence length (L_c)	Monotonically decreasing, without obvious "side lobes", with L_c of about tens of μm	Usually, with obvious "side lobes", with L_c of about tens of μm
	NOTE On average, L_c of SLD is 2–3 times less than that of ESS, the decoherence length (at the level of 0.03) of SLD is an order of magnitude smaller than that of ESS due to the absence of "side lobes"	

Excess relative intensity noise (ERIN)	**NOTE** ERIN values are comparable, SLD have slightly lower values due to an average wider spectrum	
Output polarization	Partially polarized	Nonpolarized
Service life without significant degradation of spectral parameters	10…40 thousand hours [21]	About 100 thousand hours [21]
Design features	▪ Small dimensions ▪ Relatively low efficiency of coupling to the fiber ▪ Possibility of integrating LS into compact electron-optical assemblies ▪ Commercially available devices most often come in butterfly, DIL, or similar packages	▪ The dimensions are determined by the bending radii of fibers, so ESS are usually larger than SLD ▪ They have a fiber output and, accordingly, high efficiency of coupling to the fiber

6. PROMISING AND EXPERIMENTAL LASER LS IN FOG

Despite the fact that it is difficult to build a high-precision FOG based on laser LS because of the considerable coherence length and associated parasitic interference, other parameters of laser LS, such as stability of the central wavelength and low excess noise, make it appropriate to adapt them to FOGs.

Some authors report on a successful application of a commercially available laser with distributed feedback in a tactical-grade FOG [41]. They have analyzed the source of the interferometer error and verified experimentally that the use of more advanced modern lasers, fibers, and other components of the optical scheme can reduce the contribution of parasitic effects inherent in laser LS to a level comparable to ESS, at least in tactical-grade FOGs [42].

The contribution of false interference components can be reduced by using a laser source in pulse mode [43]. Radiation in the form of short pulses significantly eliminates the effect of components caused by backscattering on the interference signal. Due to the insignificant spatial extent of short light pulses, only backscattering from a short section of the coil near its midpoint contributes to spurious interference [2, 44]. The light scattered by the rest of the coil reaches the FOG photodetector in time intervals between LS pulses, and therefore does not interfere with its signal.

In the context of application to FOGs, a logical technical solution is to artificially broaden the LS spectrum. One way is to keep the pump current of the laser diode slightly above the threshold level. The spectrum width of the laser LS in this case can be on the order of hundreds of MHz, which is sufficient to reduce the noise and parasitic components of the FOG output signal by a factor of three relative to the level achievable with a higher pump current and a spectrum width of the order of tens of MHz [45].

Another way is to use current modulation of LS, in which case it is possible to achieve spectrum broadening to 1 GHz; however, due to the relationship between the output power and the shape of the LS spectrum, the positive effect of spectrum broadening is neutralized by an increase in intensity noise and instability of the central wavelength position [45].

In [43], the use of an erbium laser with passive mode synchronization in pulsed mode in combination with light passing through a long section of a buffer fiber allowed the authors to obtain a broad spectrum common to lasers of this type when generating pulses of the order of hundreds of femtoseconds. At the same time, due to losses in the buffer fiber, nonlinear effects directly in the FOG coil can be reduced, and owing to dispersive broadening of optical pulses, such a source can be practically considered as the one operating in the continuous mode.

One of the most promising methods for broadening the spectrum relates to the field of radio photonics. A useful effect can be achieved by applying high-frequency phase modulation, formed by a pseudo-random sequence generator, to the LS [45–47]. For this purpose, an electro-optical phase modulator and a high-frequency electric signal generator are added to the FOG circuitry (Fig. 4a). Phase modulation leads to the appearance of sidebands in the optical spectrum that are symmetric relative to the optical carrier. Their heights are determined by the phase modulation amplitude, and the spectral shift relative to the carrier, by the modulation frequency. An increase in the phase modulation amplitude leads to the appearance of higher-order sidebands, the superposition of which leads to smoothing and broadening of the overall optical spectrum (Fig. 4b). The resulting spectrum width can reach 40 GHz, while maintaining the stability of the central wavelength inherent in the laser source (up to 0.15 ppm) and a low level of relative intensity noise.

The main drawback of this approach is the inevitable complication of the optical and electrical circuits of

the device, which reduces the FOG reliability and increases its final cost. Another difficulty is the need to select the mode and phase modulation parameters, which provide sufficient suppression of the optical carrier and the necessary modification of the LS spectrum.

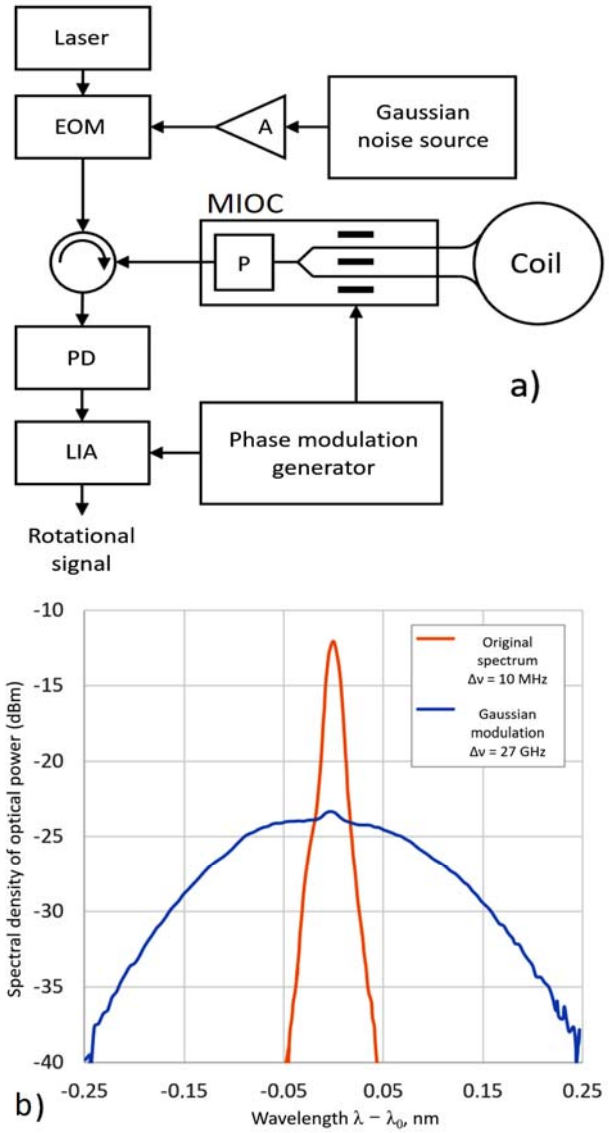

Fig. 4. Schematic of FOG with a laser LS and noise-like phase modulation, (a) A – amplifier, EOM – electro-optical modulator, LIA – lock-in amplifier, MIOC – multifunction integrated optical circuit, P – polarizer, PD – photodetector; (b) the result of the laser LS spectrum broadening, Δν – FWDM [45].

In general, it can be concluded that despite some progress in laser LS application to FOGs—mainly through artificial broadening of their spectrum— currently, they are not in demand, at least as LS for navigation-grade FOGs. Further development of methods for artificial broadening of the LS spectra is quite likely to displace SLD and ESS as the only LS in high-precision FOGs in the coming years.

7. COMMERCIALLY AVAILABLE LIGHT SOURCES OF RUSSIAN AND FOREIGN MANUFACTURERS

In order to assess the current situation in the field of development and production of LS suitable for FOGs, the authors searched and analyzed information from different foreign and domestic manufacturers of broadband LS.

In this paper, we consider the following LS produced by foreign manufacturers: SLD and ESS from FOG Photonics, Inc., Superlum (trade mark Idealphotonics), DenseLight Semiconductors, QPhotonics, LLC, Thorlabs, Anritsu (represented in Russia by company Radar), Fiberlabs Inc., Fibotec Fiberoptics GmbH, NP Photonics, Acfiber Technology Limited, OZ Optics Limited, Amonics, LD-PD Inc., Nuphoton Technologies Inc., Optilab, Xiamen Beogold Technology Co., Ltd., IRE-Polus (the Russian branch of the international company IPG Photonics Corporation), and LasersCom (Belarus) [48–66].

Among the Russian companies, the LS produced by TELAM, Nolatech, and **FORC-Photonics** may be of interest from the standpoint of their application in FOGs [67–69].

Some of the most typical LS of the above companies are shown in Figs. 5 and 6.

DL-CS5203A DenseLight Semiconuctors [50]

AS5B125EM50M Anritsu [53]

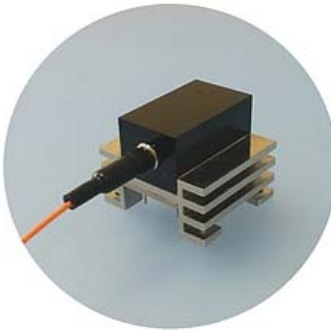

ELED-1550-1 LasersCom [65]

DL-ASE-CW-CSC117A DenseLight Semiconductors [50]

Fig. 5. Some of the most typical SLD-type LS.

Table 3 shows the main parameters of Russian and foreign LS suitable for FOGs (taking into account additional studies carried out by the authors, described in [70]).

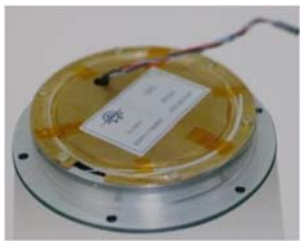

FOG Photonics SFS-1550-PM-10 [48]

Nuphoton Technologies [61]

ASE-C-20-MSA-3 Optilab [62]

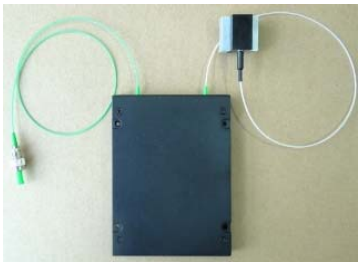

LC-ASE-C-10 LasersCom [66]

ErBBLS-35-CF-X FORC-Photonics [69]

Fig. 6. Some of the most typical ESS-type LS.

For the LS studied by the authors, Table 3 gives both the stated values /advertising data (if available) and those obtained during our studies (averaged), given in parentheses, in the second line.

In general, the results we obtained turned out to be close to the manufacturers' specifications. The differences are insignificant and can be explained by the test conditions (temperature changes, for example).

We have tested the following LS: a Nolatech SLD-1550-14BF in 14-pin butterfly package, LasersCom SLD ELED-1550-1 in 14-pin DIL package (hereinafter referred to as SLD), sources of broadband incoherent emission based on amplification of spontaneous emission LC-ASE-C-10 of the same company (hereinafter referred to as ASE), ESS-30 IRE-Polus (hereinafter referred to as ESS) and erbium fiber broadband source ErBBLS-35-CF by **FORC-Photonics** (hereinafter referred to as ErBBLS).

For the LS under consideration, we measured the emission spectra, studied the spectrum shape and width, calculated WAWs, and measured the consumed and output optical powers, also, with account for temperature dependence [70]. The LS spectral characteristics were tested with an optical spectrum analyzer. The output optical power was measured either with an appropriate power meter or embedded aids (e.g. ADC) of the source being tested.

In addition to the information given in [70], for comparison, Fig. 7 shows the plots of the emission spectra in the frequency domain of several LS tested at room temperature and the certified pump current values.

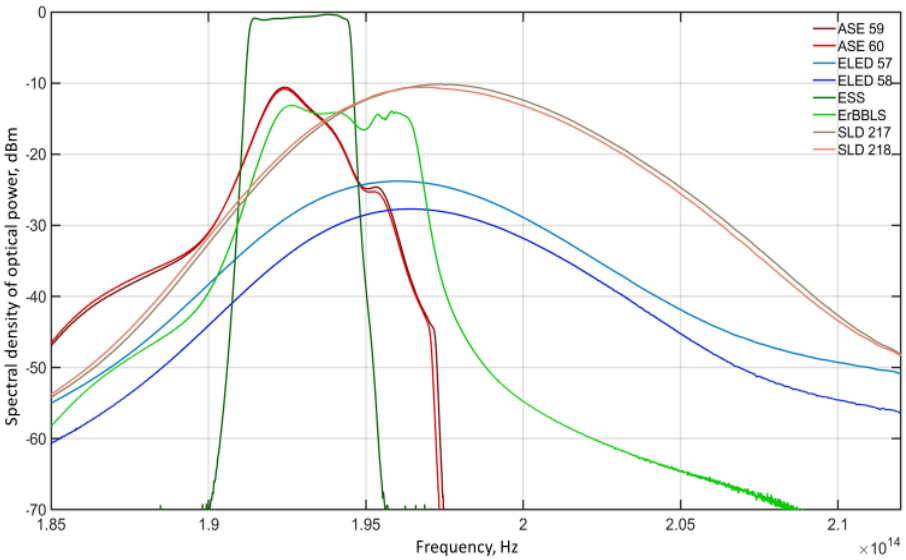

Fig. 7. Optical power spectra of several LS at room temperature and certified pump current values (according to [70]).

Table 3. Basic parameters of LS suitable for FOGs

Manufacturer	Model	LS parameters							
		Type	WAW, nm	WAW temp. coef, ppm/°C	Spectrum width (-3dB), nm	Decoherence length, mm	Output opt. power, mW	Max pumping current., мА	Working temp.range, °C
Nolatech*)	SLD-1550-14BF	SLD	1532	–	30…40	–	3…5	320±20	–40...+70
			(1521)	–	(~42)	(0.055)	(5)		
FORC-Photonics *	ErBBLs-35-CF	ESS	1546	–	~37	–	> 32	602	0...+45
			(1545)	(18)	(~35)	(~0.30)	(36)		
IRE-Polus*	ESS-30	ESS	1555	–	> 20	–	20…40	1500	0...+45
			(1554)	(3)	(~26)	(~ 0.70)	(26)		
LasersCom*	ELED-1550-1	SLD	1550	–	35…45	–	1	74.5±1	–40...+65
			(1525)	–	(~44)	(0.055)	(1)		
	LC-ASE-C-10	ESS	1560	6	11…13	–	10	100±1	–40...+60
			(1556)	(6)	(~11)	(0.25)	(10)		
TELAM	TS-1	SLD	1550	–	50	0.05	8	500	–55...+70
	TS-2	SLD	1550	–	50	0.05	15	800	–55...+70
FOG Photonics	FOG-SLD-1550-14BF	SLD	1530	–	35±5	0.07±0.01	5	300	–40...+70
	SFS-1550-PM-FA-10	ЭСИ	1550	2	>10	–	>10	–	–45...+71
SUPERLUM	SLD-761-HP1-SM-1550	SLD	1550	–	45	0.05	5	400	–55...+70
	SLD-761-HP2-SM-1550	SLD	1550	–	45	0.05	10	600	–55...+60
DenseLight Semiconductors	DL-CS5153A	SLD	1550	–	35	0.07	15	350	–40...+70
	DL-CS5203A	SLD	1550	–	35	0.07	20	450	–40...+70
	DL-CS5254A	SLD	1550	–	40	0.06	25	450	–40...+70
	DL-ASE-CW-CSC117A	SLD	1550	–	60	0.04	12.5	–	–20...+70
	DL-ASE-CW-CSC119A	SLD	1550	–	80	0.03	14	–	–20...+70
	DL-ASE-CW-CSC147A	SLD	1550	–	60	0.04	32	–	–20...+70
QPhotonics	QSDM-1550-9	SLD	1529	–	40	0.06	11	285	0...+65
	QSDM-1550-20	SLD	1567	–	61	0.04	20	707	0...+65
Thorlabs	SLD-1005S	SLD	1550	–	50	0.05	22	600	0...+65
	SLD-1550S-A40	SLD	1550	–	33	0.07	40	750	0...+65
	SLD-1550P-A40	SLD	1550	–	33	0.07	40	750	0...+65
Anritsu	AS5B125EM50M	SLD	1550	–	60	0.04	25	600	–20...+75
Fiberlabs	ASE-Md1550-25	ESS	1550	–	30	–	25	–	0…+40
Fibotec Fiberoptics	BBS-CC 14 P5 FCP	ESS	1550	–	40	–	32	–	0…+40
	BBS-CL 17 F3 FCA	ESS	1568	–	80	–	50	–	0…+40
	BBS-CL 18 W3 FCA	ESS	1568	–	80	–	63	–	0…+40
NP Photonics	ASE-C-M-7	ESS	1545	–	40	–	5	–	–
	ASE-C-M-10	ESS	1545	–	40	–	10	–	–
	ASE-C-M-13	ESS	1545	–	40	–	20	–	–
Acfiber Technology	ASE-C-M-10-G	ESS	1545	–	39	–	10	–	–20...+65
	ASE-C-M-13-G	ESS	1545	–	39	–	20	–	–20...+65
OZ Optics	ASE-11-1529:1562-S-10	ESS	1545	–	33	–	10	400	0…+40
	ASE-11-1529:1562-S-13	ESS	1545	–	33	–	20	400	0…+40
Amonics	ALS-10	ESS	1546	–	36	–	10	–	0…+60
	ALS-15	ESS	1546	–	36	–	32	–	0…+60
LD-PD	PL-LS-A-A81-PA	ESS	1550	–	40	–	10	–	–10...+50
	PL-LS-B-A81-PA	ESS	1550	–	40	–	20	–	–10...+50
Nuphoton Technologies	ASE-C0-HR-15-NA	ESS	1550	–	35	–	32	–	0...+65
	ASE-C4-MR-17-2	ESS	1550	–	35	–	50	–	0...+65
Optilab	ASE-C-20-MSA-3	ESS	1546	–	40	0.03	3x30	–	+10...+50
Xiamen Beogold Technology	BG-ASE-M1-C-1-10	ESS	1547	–	39	–	10	–	–20...+60
	BG-ASE-M1-C-1-13	ESS	1547	–	39	–	20	–	–20...+60
	BG-ASE-M1-C-1-15	ESS	1547	–	39	–	32	–	–20...+60

** Taking into account additional studies. For erbium sources, the coherence function of which has "side lobes" (see Fig. 8), the decoherence level was determined at path difference when all of the "side lobes" maxima were below 0.03. It would be more correct to specify the whole form of the coherence function for such sources in the data sheet. A dash in the boxes means that the manufacturer did not provide the data*

From the plotted spectra (using the results obtained in [70]), we calculated the WAW values (according to formula (2)), the spectrum width (at the level of –3 dB), and estimated the coherence/decoherence lengths from the coherence function plot in Fig. 8 (at 0.8 and 0.03 levels, respectively). No data on the coherence function (or the coherence/decoherence lengths for SLDs) were provided by the manufacturers of LS under consideration.

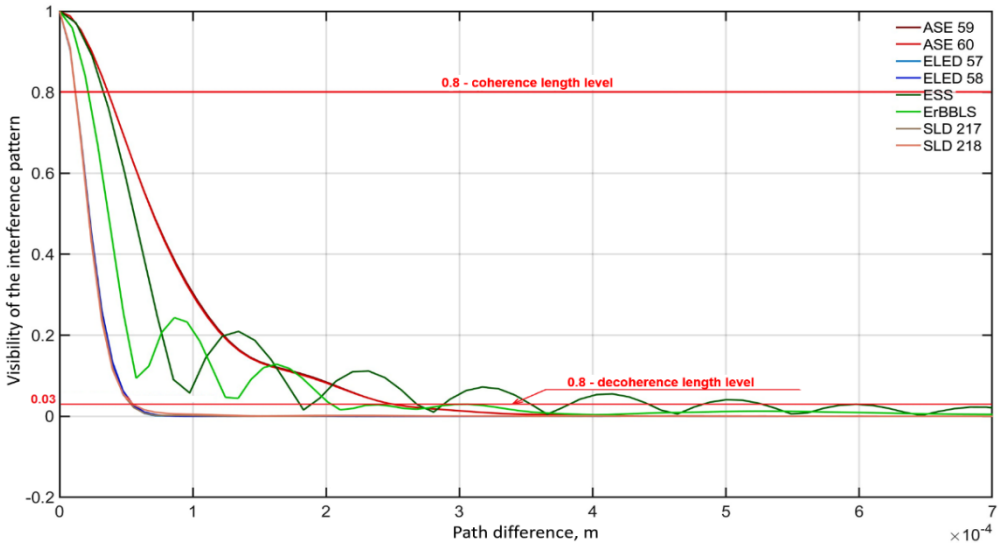

Fig. 8. Coherence functions of several LS at room temperature and certified pump current values (obtained using data from [70]).

Figures 7, A1, and A2 (see Appendix) show the typical shapes of LS spectra: Gaussian-like for SLD sources, table-shaped (in other words, close to rectangular) for erbium sources with an optical filter, also close to rectangular in shapes, but with "humps" for erbium sources without optical filters.

From Fig. 7 it can be seen that SLD and ELED, like most of the SLD sources, have a spectrum shape close to the Gaussian distribution. Their optical power ranges from 1 to 5 mW, and the spectral width reaches 35–45 nm at the level of –3 dB for SLDs, which is sufficient for use in FOGs.

ESS and ErBBLS sources have a spectrum shape close to rectangular, their spectrum width at the –3 dB level is 26–35 nm, and the optical power reaches 26–36 mW, so that one LS is sufficient to ensure the operation of three or four FOGs.

ASE sources occupy an intermediate position in terms of optical power (about 10 mW), but they are less suitable for use in FOGs because of the asymmetric shape of the spectrum and its insufficient width at the level of –3 dB (11–13 nm).

It should be noted that the spectral characteristics of the sources depend on temperature; therefore, we have also studied the temperature dependence of the main parameters of several ESS-type LS available to the authors. In particular, we studied the changes in the spectral shape for the ESS and ErBBLS sources and WAW changes due to temperature variation.

It has been found [70] that the spectrum of both sources remains rather stable with temperature variation, except for the bends in its shape at critically low (–20°C) and critically high (+70°C) temperatures. The ESS WAW is more stable than that of ErBBLS, which makes it possible to ensure higher stability of the scale factor when used in FOGs operating in a wide temperature range.

CONCLUSIONS

SLD and ESS are two types of LS used in the vast majority of modern FOGs. The choice between them is determined by the accuracy and performance requirements for a particular device.

When choosing an ESS for a FOG, it is necessary to take into account mainly the LS WAW stability, including the temperature dependence. As noted, the instability of the FOG scale factor (also under temperature variations) directly depends on the WAW instability.

The coherence length also plays an important role, but both types of LS generally have a broad spectrum and a rather small coherence length to allow this comparative criterion to be relegated to a secondary consideration.

From the information obtained and based on the results of the comparative studies, it is clear that domestic ESS are not inferior to similar foreign LS in most parameters and can be used in FOGs.

The situation with SLDs is more complicated: the choice of available models is not wide; besides, they do not have sufficient output optical power, which is significantly lower than their foreign analogues.

The appropriateness of choosing a particular source is determined by the specifics of its application, so that the information from Table 3 and the data on the emission spectra shape (Figs. A1, A2) may be useful for this purpose.

In the cases where the accuracy of the FOG being developed is not subject to strict requirements (for example, orientation or stabilization systems), but the low price of the final product, lower energy consumption and compact design are important, it makes sense to use SLD sources. At the same time, special attention should be given to the width of the operating temperature range, taking into consideration the specifics of the application.

It is also important to pay attention to the level of the output optical power (such LS are usually low-powered, so that a system with three or four FOGs may require a separate LS for each gyro).

However, if high accuracy and long service life of the product are required, and the size, power consumption and price are not so significant, then it seems appropriate to use ESS, preferably with the most stable WAW, the largest spectral width and the minimum coherence length.

Minor, yet rather important characteristics are the operating temperature range and output optical power, in particular when servicing several FOGs as part of a navigation system with a single LS.

Further development of the two main types of LS in the context of their use in different types of FOGs has several promising lines: miniaturization and embedding of LS into integrated optical assemblies; hardware and/or software stabilization of the LS spectral and energy parameters; detection, analysis and compensation for the effects caused by aging; increase of the output optical power.

Finally, the application of laser LS in FOGs, improved with radiophotonics and other methods of artificial spectrum broadening, seems promising.

APPENDIX: SPECTRUM SHAPES OF SOME ESS SPECIFIED BY MANUFACTURERS

Figure A1 shows ESS spectrum shapes specified by the manufacturers.

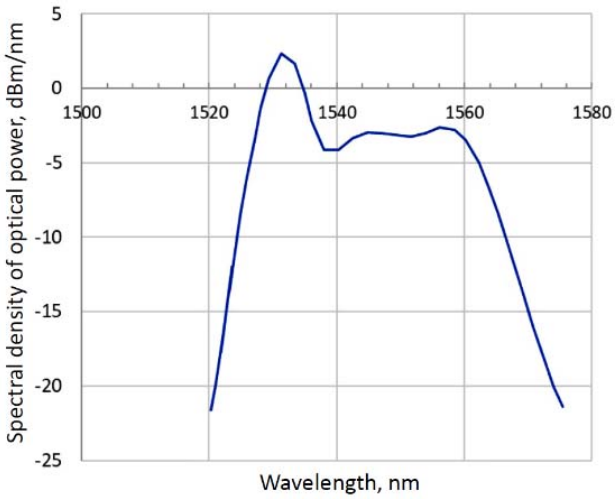

ESS ASE-Md1550-25 Fiberlabs [54]

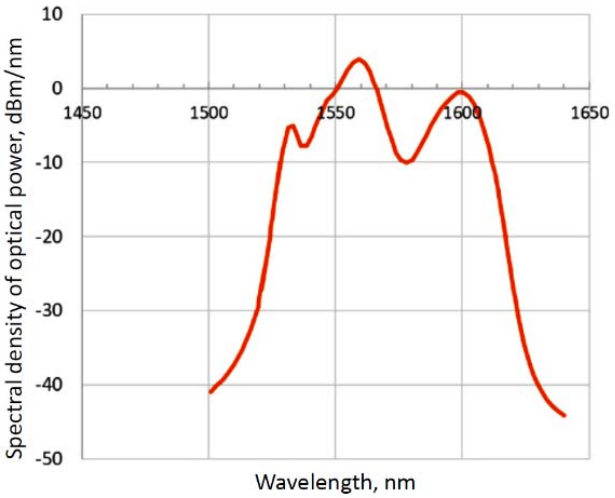

ESS Fibotec Fiberoptics [55]

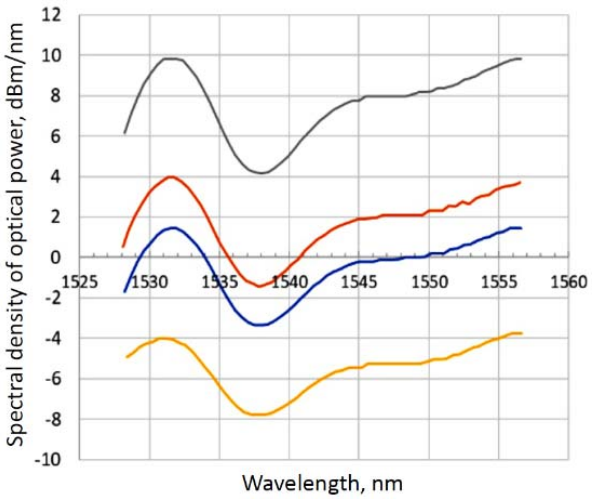

ESS Amonics [59]

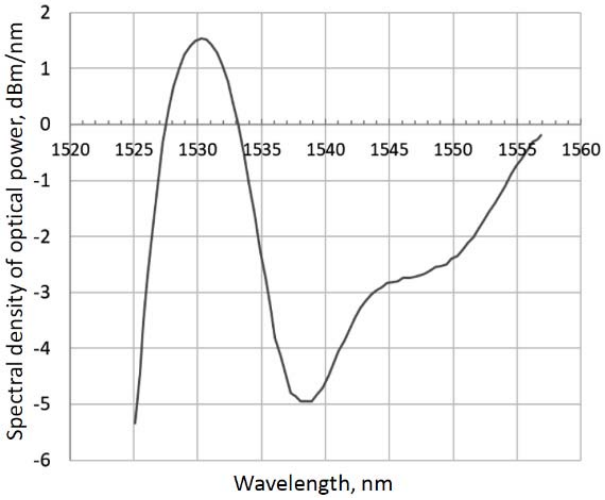

ESS ASE-C-M NP Photonics [56]

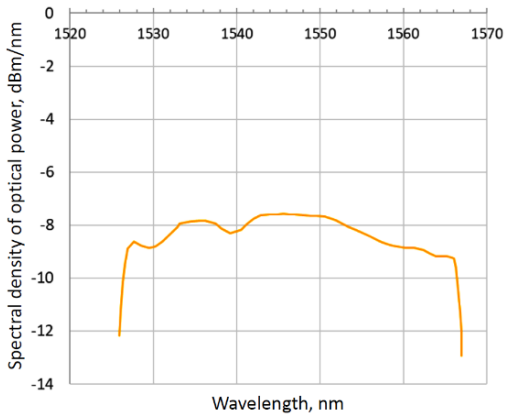

ESS ASE-C-GFF Acfiber Technology [57]

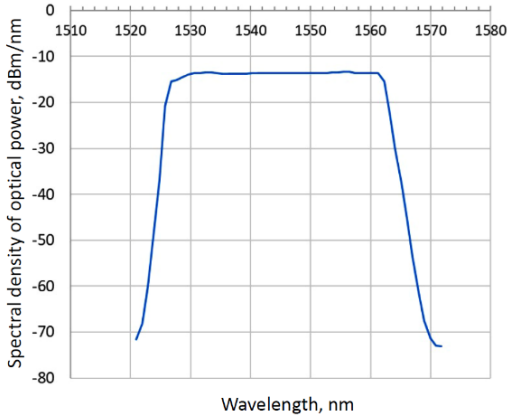

ESS ASE-11-1529:1562-S OZ Optics [58]

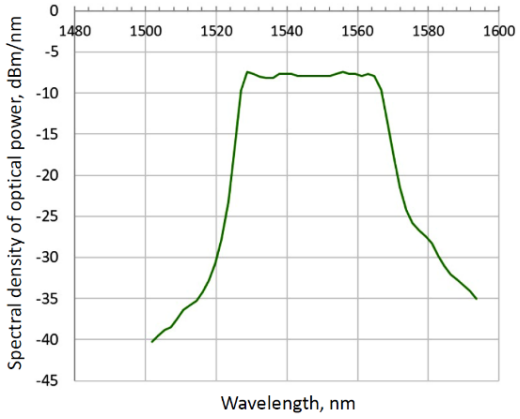

ESS PL-LS-A-A81-PA(SA) LD-PD [60]

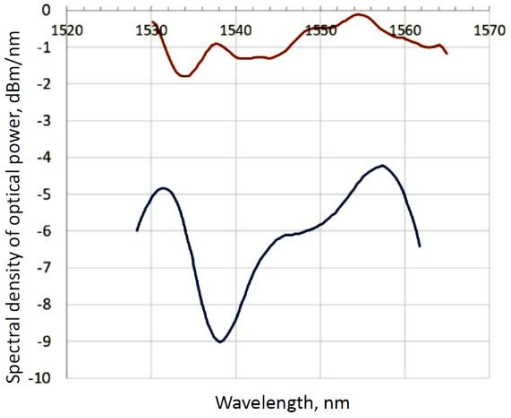

ESS from Nuphoton Technologies [61]

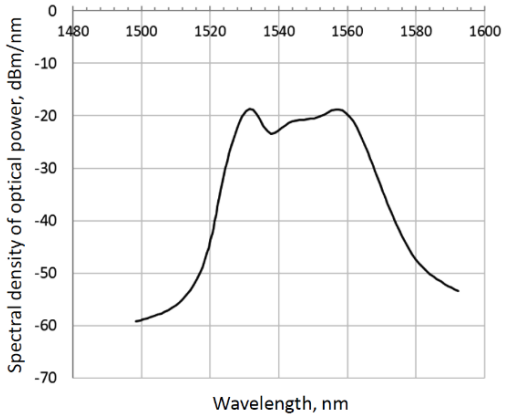

ESS ASE-C-20-MSA-3 Optilab [62]

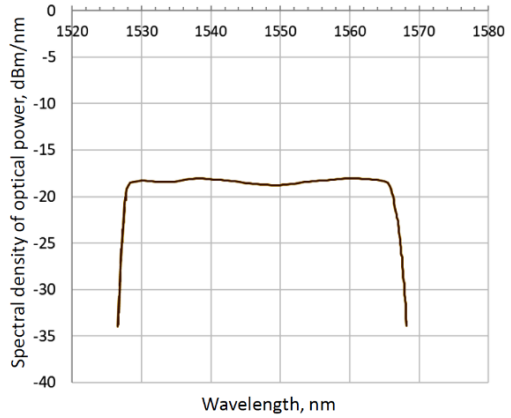

ESS BG-ASE-S-C Xiamen Beogold Tech [63]

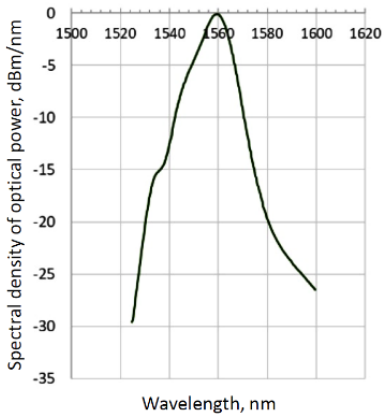

ESS LC-ASE-C-10 LasersCom [66]

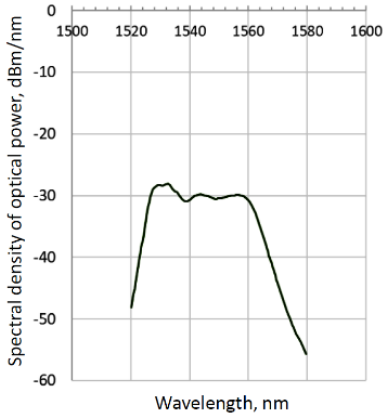

ESS ErBBLS-35-CF-X НЦВО Фотоника [69]

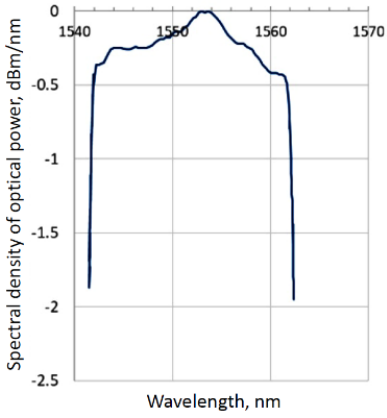

ESS ESS-30 ИРЭ-Полюс [64]

Fig. 1A. ESS spectrum shapes specified by the manufacturers.

Figure A2 shows SLD spectrum shapes specified by the manufacturers. For SLD-761-HP2-SM-1550 from Superlum [49], the manufacturer also provided information about the intrinsic LS spectrum pulsation.

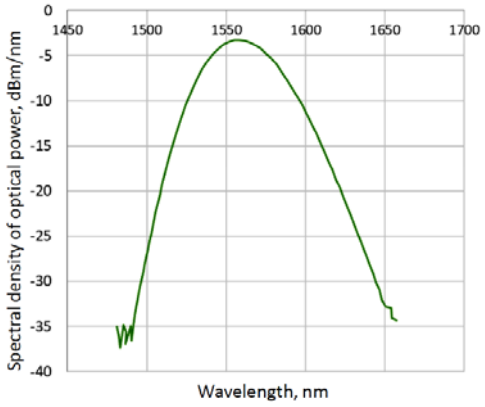

FOG-SLD-1550-14BF FOG Photonics [48]

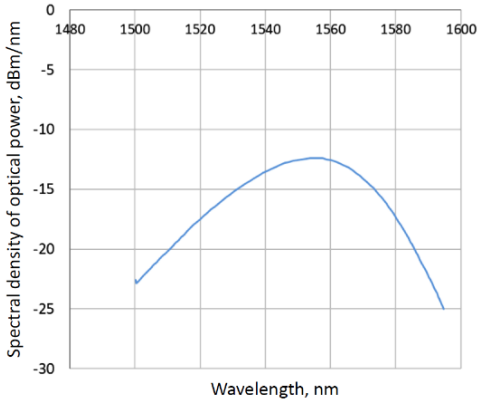

SLD DL-CS5203A DenseLight Semiconductors [50]

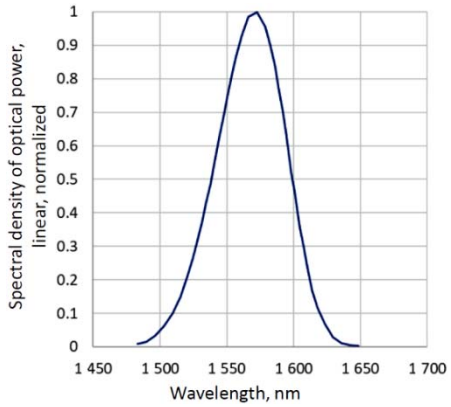

SLD QSDM-1550-20 QPhotonics [51]

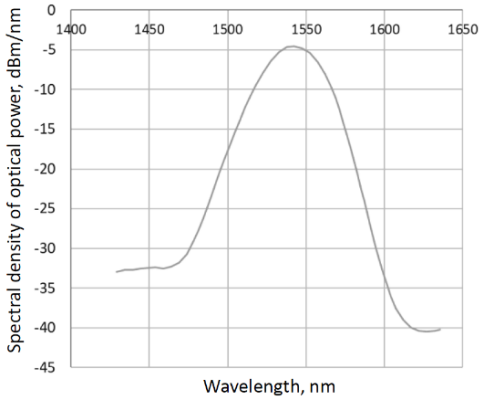

SLD SLD1550P-A40 Thorlabs [52]

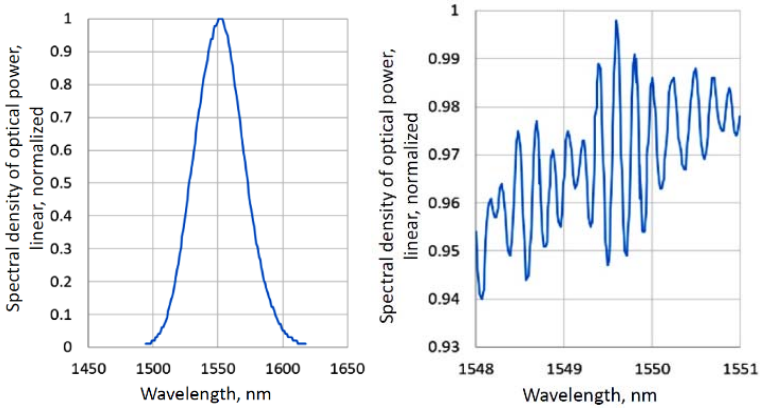

Spectrum and intrinsic spectrum pulsation
SLD SLD-761-HP2-SM-1550 Superlum [49]

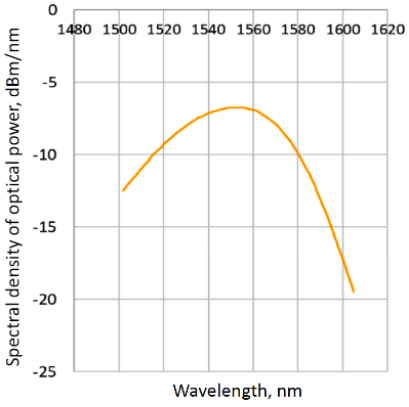

DL-ASE-CW-CSC117A
DenseLight Semiconductors [50]

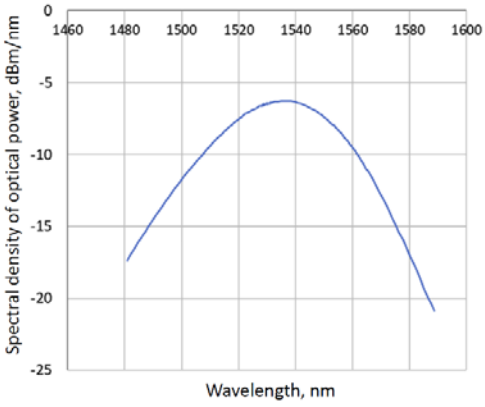

ELED-1550-1 LasersCom [58]

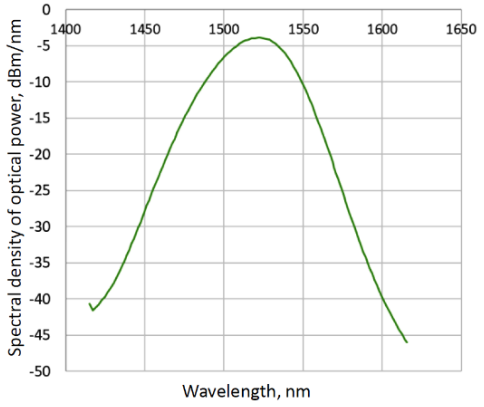

SLD SLD-1550-14BF from Nolatech [61, 63]

Fig. A2. SLD spectrum shapes specified by the manufacturers.

Note: Nolatech's website does not provide LS spectra shapes; the graph in the figure was obtained by the authors at the rated pump current [70].

ACKNOWLEDGMENTS

We are grateful to V.E. Strigalev for careful reading of the manuscript and helpful remarks.

FUNDING

This work was supported by ongoing institutional funding. No additional grants to carry out or direct this particular research were obtained.

CONFLICT OF INTEREST

The authors of this work declare that they have no conflicts of interest.

REFERENCES

1. Peshekhonov, V.G., The outlook for gyroscopy, Gyroscopy and Navigation, 2020, vol. 11, pp. 193–197. https://doi.org/10.1134/S2075108720030062
2. Lefevre, H.C., The Fiber Optic Gyroscope, 3rd ed., Norwood: Artech House Publishers, 2022.
3. Lefevre, H.C., The fiber-optic gyroscope, a century after Sagnac's experiment: The ultimate rotation-sensing technology? Comptes Rendus Physique, 2014, vol. 15, issue 10, pp. 851–858, DOI 10.1016/j.crhy.2014.10.007.
4. Takada, K., Calculation of Rayleigh backscattering noise in fiber-optic gyroscopes, Journal of the Optical Society of America A, 1985, vol. 2, issue 6, pp. 872–877.
5. Salekh, B. and Teikh, M., Optika i fotonika. Printsipy i prilozheniya: uchebnik (Optics and photonics. Principles and applications), vol. 2, Dolgoprudnyi: Izdatel'stvo Intellekt, 2012.
6. Strigalev, V.E., Meshkovskii, I.K., and Moor, Ya.D., Osobennosti primeneniya fazochuvstvitel'nykh ustroistv v volokonno-opticheskikh izmeritel'nykh priborakh (Features of Using Phase-Sensitive Devices in Fiber-Optic Measuring Systems), St. Petersburg: ITMO University, 2021.
7. Aleinik, A.S., Kikilich, N.E., Kozlov, V.N., Vlasov, A.A., and Nikitenko, A.N., Methods for constructing high-stable erbium superluminescent fiber sources, Nauchno-tekhnicheskii vestnik informatsionnykh tekhnologii, mekhaniki i optiki, 2016, vol. 16, no. 4 (104), pp. 593–607.
8. Hakimi, F. and Moores, J.D., RIN-reduced light source for ultra-low noise interferometric fibre optic gyroscopes, Electronics Letters, 2013, vol. 49, no. 3. DOI https://doi.org/10.1049/el.2012.3371.
9. Guattari, F., Chouvin, S., Molucon, C., et al., A simple optical technique to compensate for excess RIN in a fiber-optic gyroscope, Inertial Sensors and Systems 2014, Karlsruhe, Germany, 2014, p.10.
10. Aleinik, A.S., Deineka, I.G., Smolovik, M.A., Neforosnyi, S.T., and Rupasov, A.V., Compensation for excess RIN in fiber-optic gyro, Gyroscopy and Navigation, 2016, vol. 7, no. 3, pp. 214-222.
11. Wysocki, P.F., Digonnet, M.J.F., Kim, B.Y., Shaw, H.J., Characteristics of erbium-doped superfluorescent fiber sources for interferometric sensor applications, Journal of Lightwave Technology, 2009, vol. 12, issue 3, pp. 550–567.
12. Park, H.G., Digonnet, M.J.F., and Kino, G., Er-Doped Superfluorescent Fiber Source With a ±0,5-ppm Long-Term Mean-Wavelength Stability, Journal of Lightwave Technology, 2003, vol. 21, no. 12. DOI 10.1109/JLT.2003.822539.
13. Ashley, P.R., Temmen, M.G., and Sanghadasa, M., Applications of SLDs in fiber optical gyroscopes, Proc. SPIE – The International Society for Optical Engineering, 2002, no. 4648, pp. 104–115.
14. Zheng, S., Ren, M., Luo, X., Zhang, H., and Feng, G., Real-Time Compensation for SLD Light-Power Fluctuation in an Interferometric Fiber-Optic Gyroscope, Sensors, 2023, no. 23 (4), p. 1925.
15. Chen, X., Yang, J., Zhou, Y., Shu, X., An improved temperature compensation circuit for SLD light source of fiber-optic gyroscope, Journal of Physics: Conference Series, 2017, no. 916(1), p. 012027.
16. Vostrikov, E., Kikilich, N., Zalesskaya, Y., Aleinik, A., Smolovik, M., Deyneka, I., and Meshkovskii, I., Stabilisation of central wavelength of erbium-doped fibre source as part of high-accuracy fibre optic gyroscopes, IET Optoelectronics, 2021, no. 15(6), pp. 287–293. DOI 10.1049/ote2.12040.
17. Li, X., Li, M., Liu, C., Li, H., and Yang, H., Research on light source average wavelength and crystal oscillator frequency for reducing temperature error of the FOG scale factor, Optik – International Journal for Light and Electron Optics, 2021, no. 242, p. 167189, DOI 10.1016/j.ijleo.2021.167189.
18. Chen, X., Yan, M., Yu, J., and Tang, R., Design of light source for ultrahigh precision fiber optic gyroscope, Proc. SPIE 12062, AOPC 2021: Optoelectronics and Nanophotonics, 1206211 (21 December 2021). DOI 10.1117/12.2607120.
19. Alphonse, G.A., Hawrylo, F.Z., and Harvey, M., Super-luminescent diode. U.S. Patent No. 4,821,276, 1989.
20. Chen, X., Jiang, L., Yang, M., Yang, J., and Shu, X., Research on the mean-wavelength drift mechanism of SLD light source in FOG, IOP Conf. Series: Journal of Physics: Conf. Series 1300, 2019, 012047.
21. Andreeva, E.V., Il'chenko, S.N., Kostin, Yu.O., Lapin, P.I., Mamedov, D.S., and Yakubovich, S.D., Changes in the output characteristics of broadband superluminescent diodes during long-term operation, Kvantovaya elektronika, 2011, vol. 47, no. 7, pp. 595–601.
22. Hsiao, C., Fang, Y., Chen, Y., Weng, Z., Chu, J., Chen, R., Dong, C., Lin, W., and Chiu, Y., Fabrication of superluminescent diode (SLD) for gyro light source with broadband, high power, and large polarization-extinction ratio performance, Opto-Electronics and Communications Conference (OECC), 2020, pp. 1–3 DOI 10.1109/OECC48412.2020.9273634.
23. Chen, X., Yang, J., Zhang, C., Yang, M., and Jiang, L., The application of intelligent modelling system in temperature compensation of SLD light source, Proc. SPIE 11023, Fifth Symposium on Novel Optoelectronic Detection Technology and Application, 110234Z (12 March 2019). DOI 10.1117/12.2520493.
24. Chen, X., Yang, J., Zhou, Y., and Shu, X., An improved temperature compensation circuit for SLD light source of fiber-optic gyroscope, IOP Conf. Series: Journal of Physics: Conf. Series 916, 2017, 012027.

25. Shang, K., Lei, M., Xiang, Q., Na, Y., Zhang, L., and Yu, H., Near-navigation-grade interferometric fiber optic gyroscope with an integrated optical chip, Chinese Optics Letters, 2020, vol. 18, issue 12, p. 120601.
26. Li, X., Shao, Z., Lu, J., Yuan, H., Gao, B., and Gao, H., Study of high-performance fiber optic gyroscope based on SLD light source, 25th Chinese Control and Decision Conference (CCDC), Guiyang, China, 2013, pp. 1459–1463. DOI: 10.1109/CCDC.2013.6561156.
27. Optolink LLC. http://www.optolink.ru. Accessed April 03, 2024.
28. Fizoptika. https://www.fizoptika.ru. Accessed April 03, 2024.
29. KVH Industries, Inc. https://www.kvh.com. Accessed April 03, 2024.
30. Kikilich, N.Ye., Stabilization of the parameters of a superluminescent fiber source for use in a fiber-optic gyroscope, Cand. Sci. (Technology), St.Petersburg, 2018, p. 138.
31. Huang, Y., Peng, T., Wang, L., Liu, R., Performance comparison of fiber-optic gyroscopes using single pass backward and double pass backward superfluorescent fiber sources, Proc. SPIE – The International Society for Optical Engineering, 2009, no. 7503.
32. Falquier, D.G., Wagener, J.L., Digonnet, M.J.F., Shaw, H.J., Polarized Superfluorescent Fiber Sources, Optical Fiber Technology, 1998, 4, 453–470, Article No. OF98T0260.
33. CSRayzer Optical Technology. https://www.csrayzer.cn. Accessed April 03, 2024.
34. Lumispot Technology Group. https://www.lumispot-tech.com. Accessed April 03, 2024.
35. Aubry, M., Mescia, L., Morana, A., Robin, T., Laurent, A., Mekki, J., Marin, E., Ouerdane, Y., Girard, S., Boukenter, A., Temperature Influence on the Radiation Responses of Erbium-Doped Fiber Amplifiers, Phys. Status Solidi A, 2021, 2100002. DOI 10.1002/pssa.202100002.
36. Wan, S., Zhan, T., Hu, D., Yan, H., Han, D., An Erbium-doped fiber source with near-Gaussian-shaped spectrum based on double-stage energy matching and LPFGs, Photonics, 2023, no. 10(5), p. 533.
37. Concern CSRI Elektroprobor. http://www.elektropribor.spb.ru. Accessed October 03, 2023.
38. Perm Scientific-Industrial Instrument Making Company (PNPPK) https://pnppk.ru. Accessed October 03, 2023.
39. Exail Company. https://www.exail.com. Accessed October 03, 2023.
40. Northrop Grumman Corporation. https://www.northropgrumman.com. Accessed October 03, 2023.
41. Lloyd, S.W., Digonnet, M.J.F., Fan, S., Tactical-grade interferometric fiber optic gyroscope driven with a narrow-linewidth laser, Advanced Photonics, OSA Technical Digest (CD) Optica Publishing Group, 2011, SMC3.
42. Lloyd, S.W., Digonnet, M.J.F., Fan, S., Modeling Coherent Backscattering Errors in Fiber Optic Gyroscopes for Sources of Arbitrary Line Width, Journal of Lightwave Technology, 2013, vol. 31, no. 13, July 1. DOI 10.1109/JLT.2013.2261283.
43. Chou, P.C., Haus, H.A., Laznicka, O.M., Pulse excited interferometric fiber-optic gyroscope, CLEO'98, pp. 313–314.
44. Cutler, C.C., Newton, S.A., Shaw, H.J., Limitation of rotation sensing by scattering, Optics letters, 1980, vol. 5, no. 11, pp. 488–490. DOI 10.1364/OL.5.000488.
45. Chamoun, J., Digonnet, M.J.F., Aircraft-navigation-grade laser-driven FOG with Gaussian-noise phase modulation, Optic Letters, 2017, vol. 42, no. 8, pp. 1600–1603.
46. Wheeler, J.M., Chamoun, J.N., Digonnet, M.J.F., Optimizing Coherence Suppression in a Laser Broadened by Phase Modulation with Noise, Journal of Lightwave Technology, 2021, vol. 39, no. 9, pp. 2994–3001, DOI 10.1109/JLT.2021.3061938.
47. Yan, J., Miao, L., Shen, H., Shu, X., Huang, T., Che, S., Low-Drift Closed-Loop Fiber Optic Gyroscope of High Scale Factor Stability Driven by Laser with External Phase Modulation, Photonic Sensors, 2022, vol. 12, issue 3, id. 220304.
48. FOGphotonics, Inc. http://www.fogphotonics.com. Accessed April 03, 2024.
49. Superlum Company. https://www.superlumdiodes.com. Accessed April 03, 2024.
50. DenseLight Semiconductors. https://www.denselight.com. Accessed April 03, 2024.
51. QPhotonics, LLC. https://www.qphotonics.com. Accessed April 03, 2024.
52. Thorlabs Inc. https://www.thorlabs.com. Accessed April 03, 2024.
53. Anritsu Company. https://www.anritsu.com. Accessed April 03, 2024.
54. Fiberlabs Inc. https://www.fiberlabs.com. Accessed April 03, 2024.
55. Fibotec Fiberoptics. https://www.fibotec.com. Accessed April 03, 2024.
56. NP Photonics. http://www.npphotonics.com. Accessed April 03, 2024.
57. Acfiber Technology Limited. https://www.acfiber.com. Accessed April 03, 2024.
58. OZ Optics Limited. https://www.ozoptics.com. Accessed April 03, 2024.
59. Amonics Company. https://www.amonics.com. Accessed April 03, 2024.
60. LD-PD Inc. http://ld-pd.com. Accessed April 03, 2024.
61. Nuphoton Technologies Inc. https://nuphoton.com. Accessed April 03, 2024.
62. Optilab Company. https://www.optilab.com. Accessed April 03, 2024.
63. Xiamen Beogold Technology Co., Ltd.: https://www.beogold.com. Accessed April 03, 2024.
64. Scientific and Technical Association IRE-Polus. ESS-30 assembly protocol. Test results, 2018.
65. LASERSCOM. Superluminescent diode ELED-1550-1. https://laserscom.com/sites/default/files/pdf/eled-1550-1_0.pdf. Accessed April 03, 2024.
66. LASERSCOM. Superluminescent fiber source LC-ASE-C-10. https://laserscom.com/sites/default/files/pdf/lc-ase-c-10_1.pdf. Accessed April 03, 2024.
67. TELAM http://telam.ru Accessed April 03, 2024.
68. NOLATECH. http://nolatech.ru. Accessed April 03, 2024.
69. FORC-Photonics. https://www.forc-photonics.ru. Accessed April 03, 2024.
70. Egorov, D.A. and Klyuchnikova, E.L., Results of comparative study of light sources for fiber optic gyroscopes, Gyroscopy and Navigation, 2022, vol. 13, no. 4, pp. 304–309. https://doi.org/10.1134/S2075108722040046